

Statins Impair Glucose Uptake in Tumor Cells¹

Agata Malenda^{*}, Anna Skrobanska^{*},
Tadeusz Issat^{*}, Magdalena Winiarska^{*},
Jacek Bil^{*}, Bozenna Oleszczak[†], Maciej Sinski[‡],
Małgorzata Firczuk^{*}, Janusz M. Bujnicki^{§,¶},
Justyna Chlebowska^{*}, Adam D. Staruch^{*},
Eliza Glodkowska-Mrowka^{*}, Jolanta Kunikowska[#],
Leszek Krolicki[#], Leszek Szablewski[†],
Zbigniew Gaciong[‡], Katarzyna Kozia^{**},
Marek Jakobisiak^{*}, Jakub Golab^{*,††}
and Dominika A. Nowis^{*}

^{*}Department of Immunology, Center of Biostructure Research, Medical University of Warsaw, Warsaw, Poland;

[†]Center of Biostructure Research, Medical University of

Warsaw, Warsaw, Poland; [‡]Department of Internal

Diseases, Hypertension and Vascular Disease, Medical University of Warsaw, Warsaw, Poland; [§]Laboratory of

Bioinformatics and Protein Engineering, International Institute of Molecular and Cell Biology in Warsaw, Warsaw, Poland;

[¶]Bioinformatics Laboratory, Institute of Molecular Biology and Biotechnology, Adam Mickiewicz University, Poznan, Poland;

[#]Nuclear Medicine Department, Medical University of Warsaw, Warsaw, Poland; ^{**}Department of

General and Nutritional Biochemistry, Medical University of Warsaw, Warsaw, Poland; ^{††}Institute of Physical Chemistry, Polish Academy of Sciences, Department 3, Warsaw, Poland

Abstract

Statins, HMG-CoA reductase inhibitors, are used in the prevention and treatment of cardiovascular diseases owing to their lipid-lowering effects. Previous studies revealed that, by modulating membrane cholesterol content, statins could induce conformational changes in cluster of differentiation 20 (CD20) tetraspanin. The aim of the presented study was to investigate the influence of statins on glucose transporter 1 (GLUT1)-mediated glucose uptake in tumor cells. We observed a significant concentration- and time-dependent decrease in glucose analogs' uptake in several tumor cell lines incubated with statins. This effect was reversible with restitution of cholesterol synthesis pathway with mevalonic acid as well as with supplementation of plasma membrane with exogenous cholesterol.

Abbreviations: 2-DOG, 2-deoxyglucose; 6-NBDG, 6-(*N*-(7-nitrobenz-2-oxa-1,3-diazol-4-yl)amino)-6-deoxyglucose; CD, cluster of differentiation; CRAC, cholesterol recognition/interaction amino acid consensus; ¹⁸F-FDG, [¹⁸F]fluoro-2-deoxyglucose; FPP, farnesyl pyrophosphate; GLUT, glucose transporter; HA, hemagglutinin; MA, mevalonic acid; MβCD, methyl-β-cyclodextrin; PBMC, peripheral blood mononuclear cell; PET/CT, positron emission tomography/computed tomography; SUV, standardized uptake value
Address all correspondence to: Dominika A. Nowis, MD, PhD, Department of Immunology, Center of Biostructure Research, The Medical University of Warsaw, 1a Banacha Str., F Bldg, 02-097 Warsaw, Poland. E-mail: dominika.nowis@wum.edu.pl

¹J.G., A.M., and D.N. are recipients of the Mistrz Award from the Foundation for Polish Science. J.G., M.W., and M.F. are members of TEAM Programme co-financed by the Foundation for Polish Science and the EU European Regional Development Fund. The research was supported by grants 1M19/NM1 (to A.M.), 1M19/NM6 (to A.M.), and 1W13/W1/10 (to L.K.) from the Medical University of Warsaw, N N402 365438 (to J.G.), N N405 302836 (to M.J.) from Polish Ministry of Science, the European Union within European Regional Development Fund through Innovative Economy grant POIG.01.01.02-00-008/08 (to J.G.) as well as by grant N R13 0094 06 (to K.K.) from The National Centre for Research and Development. The work carried out by J.M.B. (modeling of GLUT1) was supported by the 7th Framework Programme of the European Commission (EC FP7, grant HEALTHPROT, contract number 229676). None of these organizations had any influence neither on the course of the studies nor on the preparation of the article.

Received 26 February 2012; Revised 22 March 2012; Accepted 22 March 2012

Statins did not change overall GLUT1 expression at neither transcriptional nor protein levels. An exploratory clinical trial revealed that statin treatment decreased glucose uptake in peripheral blood leukocytes and lowered ^{18}F -fluorodeoxyglucose (^{18}F -FDG) uptake by tumor masses in a mantle cell lymphoma patient. A bioinformatics analysis was used to predict the structure of human GLUT1 and to identify putative cholesterol-binding motifs in its juxtamembrane fragment. Altogether, the influence of statins on glucose uptake seems to be of clinical significance. By inhibiting ^{18}F -FDG uptake, statins can negatively affect the sensitivity of positron emission tomography, a diagnostic procedure frequently used in oncology.

Neoplasia (2012) 14, 311–323

Introduction

Owing to the deregulated blood supply, rapidly growing tumor cells suffer from lack of oxygen and nutrients. An increased glucose metabolism seems to be an important mechanism of tumor cells adapting to hypoxia. Intriguingly, transformed cells tend to use anaerobic glycolysis as their major energy supply even under normoxic conditions such as during cell culture. Although glycolysis is less efficient in generating ATP than oxidative phosphorylation (tricarboxylic acid cycle), it is much faster and provides substrates to the synthesis of amino acids, nucleotides, and fatty acids as well as reduces equivalents to minimize toxic effects of reactive oxygen species [1,2]. The shift in ATP generation from oxidative phosphorylation to glycolysis even under normal oxygen conditions is called the Warburg effect. It seems that the first regulatory step in glycolysis, that is, the increased glucose uptake, is the biologic basis for the diagnostic procedure of [^{18}F] fluoro-2-deoxyglucose positron emission tomography (FDG PET) [3,4]. Although various mechanisms have been proposed to explain increased FDG uptake in growing tumors, a facilitative glucose transport by glucose transporters (GLUTs) seems to be the most important [5–7]. GLUT family includes 14 isoforms sharing common structural features including 12 transmembrane domains with both amino- and carboxy-terminal ends localized in the cytoplasm [8]. GLUT1 is frequently upregulated in tumor cells, which probably facilitates tumor growth beyond the size limited by their glycolytic capacity [9]. A number of studies indicate that increased GLUT1 expression correlates with higher tumor ^{18}F -FDG uptake [10–12].

We have previously demonstrated that statins, which are the 3-hydroxy-3-methylglutaryl coenzyme A reductase inhibitors, can induce conformational changes in CD20 molecules. This results in impaired binding of anti-CD20 monoclonal antibodies and diminished ability to trigger complement-dependent cytotoxicity [13]. These effects turned out to be strictly cholesterol dependent because exogenous cholesterol could rapidly reverse the effects of statins. Atomic force microscopy, limited proteolysis, and functional data indicated that statins induced cholesterol-dependent conformational changes in CD20 tetraspanin. We hypothesized that statins could also induce conformational changes in other proteins with multiple membrane-spanning domains. Such possibility is also supported by a number of observations indicating that statins or membrane cholesterol depletion impairs the function of other proteins with multiple membrane-spanning domains including P-glycoprotein [14], P2X₁-4 ATP receptors [15], voltage-gated chloride channel [16], G-protein-coupled cholecystokinin [17], or serotonin receptors [18]. Modeling of the serotonin_{1A} receptor revealed that, in the presence of cholesterol, the receptor acquires a more compact

structure, and its ligands exhibit higher binding energies when docked to the receptor in the presence of cholesterol [19]. A recent study that used small-angle neutron scattering revealed that cholesterol-rich micellar nanostructures determine transmembrane protein (GPCR) activity and that successful reconstitution of the receptor is dependent on cholesterol-protein interactions [20]. Moreover, cholesterol-binding motifs have recently been characterized in acetylcholine receptors, which contain five transmembrane domains [21]. Therefore, we decided to investigate the influence of statins on the glucose transport into tumor cells, which frequently overexpress GLUT proteins and require efficient glucose uptake for their increased metabolic demands.

Materials and Methods

Cell Culture

Human Burkitt lymphoma (Daudi, Raji, Ramos), human follicular lymphoma (DoHH2), human colon adenocarcinoma (LoVo), and human embryonic kidney (HEK293T) cell lines were purchased from the American Tissue Culture Collection (Manassas, VA). Cells (Daudi, Raji, Ramos, DoHH2, and HEK293T) were cultured in RPMI 1640 or Dulbecco modified Eagle medium/F-12 medium (LoVo) supplemented with 10% heat-inactivated fetal bovine serum, 100 $\mu\text{g}/\text{ml}$ streptomycin, and 250 ng/ml amphotericin B (all from Invitrogen, Carlsbad, CA). Cells were cultured at 37°C in a fully humidified atmosphere of 5% CO₂ and were passaged approximately every other day.

Reagents

The following statins were used: atorvastatin (Pfizer Pharmaceuticals, Inc, Groton, CT), cerivastatin (Bayer Corp, West Haven, CT), fluvastatin (Novartis Pharma AG, Basel, Switzerland), lovastatin, and simvastatin (both from Merck, Sharp & Dohme Res. Lab., Rahway, NJ). Lovastatin and simvastatin were obtained in the inactive lactone form. They were converted to the active form by dissolving in ethanol, heating for 2 hours at 50°C in 0.1N NaOH and neutralizing with HCl. Distilled water was added to obtain the final stock concentration of 10 mM. Stock solution was aliquoted and stored frozen (–20°C). Mevalonic acid (MA), farnesyl pyrophosphate (FPP), methyl- β -cyclodextrin (M β CD), and water-soluble cholesterol were purchased from Sigma (St Louis, MO). Farnesyltransferase inhibitor L-744,832 was obtained from Merck KGaA (Darmstadt, Germany); 6-(*N*-7-nitrobenz-2-oxa-1,3-diazol-4-yl)amino)-6-deoxyglucose (6-NBDG) was from Invitrogen and was dissolved in dimethyl sulfoxide to

10-mM stock concentration; 4,6-ethylidine-D-glucose (ETDG) was purchased from Sigma.

Flow Cytometry

For flow cytometry studies, 5×10^5 cells were resuspended in 300 μ l of phosphate-buffered saline (PBS) and incubated with 300 μ M 6-[N-(7-nitrobenz-2-oxa-1,3-diazol-4-yl)amino]-6-deoxyglucose (6-NBDG) or with anti-hemagglutinin (HA) phycoerythrin (PE)-conjugated monoclonal antibody (Miltenyi Biotec, Bergischgladbach, Germany; 1:10 dilution) or PE-conjugated immunoglobulin G1 (Beckman Coulter, Miami, FL; 1:10 dilution), which served as an isotypic control, for 30 minutes at room temperature in dark. As a control of glucose uptake, 200 mM ETDG was used. Before analysis, cells were washed twice with PBS and resuspended in 300 μ l PBS. Additional staining with 2.5 μ g/ml propidium iodide (Sigma-Aldrich) was performed to distinguish dead cells. The cells were analyzed on FACS Scan flow cytometer (Becton Dickinson, Franklin Lakes, NJ) using CellQuest Pro Software Version 5.2. 6-NBDG uptake was identified by gating the viable (propidium iodide [PI]-negative) cells. The mean fluorescence intensity (MFI) served as a measure for 6-NBDG uptake on a per-cell basis.

Radioisotope Measurement of Glucose Uptake

For the evaluation of [1,2-³H]-deoxy-D-glucose (2-DOG; Perkin-Elmer, Waltham, MA) uptake, the protocol of Kaliman et al. [22] was used with minor modifications. Briefly, 3×10^5 cells resuspended in 300 μ l of transport solution (20 mM HEPES, 150 mM NaCl, 5 mM KCl, 5 mM MgSO₄, 1.2 mM KH₂PO₄, 25 mM CaCl₂, 2 mM pyruvate, pH 7.4) were incubated for indicated time with 1.5 μ l of 2-DOG (8.0 mCi/ml radionuclide concentration). 2-DOG uptake was stopped by adding 50 mM D-glucose solution in PBS at 4°C. After a three-time wash in PBS, the cells were lysed with 0.1 M NaOH + 0.1% SDS solution and left overnight at 4°C to enable proper cell lysis. To evaluate the nonspecific uptake of isotope-labeled deoxy-D-glucose (time t_0), a stop solution (50 mM of D-glucose in PBS) was added to the cellular suspension instead of the PBS solution. The following day, the lysates were analyzed in a scintillation counter (Wallac, Gaithersburg, MD). All experimental groups were performed in duplicates. The values presented net uptake per 3×10^5 cells of label, which is the total label accumulated at given time minus the radioactivity bound to the surface of the cells (time t_0).

Cell Cycle Analysis

For the cell cycle analysis, 5×10^5 cells were fixed for 1 hour in ice-cold 70% ethanol, washed twice with PBS, digested for 10 minutes with 100 μ g/ml RNase A (Qiagen, Chatsworth, CA) and stained with 5 μ g/ml propidium iodide (Sigma). Next, the cells were analyzed with FACS Scan flow cytometer using CellQuest Pro Software Version 5.2.

G₁, S, and G₂/M phases of the cell cycle were distinguished according to the cellular DNA content ($\leq 2n$; $(2n-4n)$, $\geq 4n$, respectively).

Lactate Concentration Measurements

Lactate concentration in cell culture supernatants was estimated electrochemically using lactate oxidase method on ABL Radiometer ABL 800 FLEX blood gas analyzer (Radiometer Medical ApS, Brønshøj, Denmark). Values obtained were normalized for total cellular protein concentration.

Western Blot Analysis

Control or drug-treated cells were washed twice with PBS, pelleted, and lysed with 25 mM HEPES, 0.3 M NaCl, 1.5 mM MgCl₂, 20 mM β -glycerol-phosphate, 2 mM EDTA, 2 mM EGTA, 1 mM dithiothreitol, 1% Triton X-100, and 10% glycerol-containing buffer supplemented with Complete protease inhibitor cocktail (Roche Diagnostics, Basel, Switzerland). Protein concentration was measured using Bio-Rad Protein Assay (Bio-Rad, Hercules, CA). Equal amounts of whole-cell proteins were separated on 10% SDS-polyacrylamide gel, transferred onto Protran nitrocellulose membranes (Schleicher & Schuell BioScience, Keene, NH), blocked with Tris-buffered saline (pH 7.4) and 0.05% Tween 20 supplemented with 5% bovine serum albumin. Anti-GLUT1 (Millipore, Temecula, CA) rabbit polyclonal antibody at 1:1000 dilution was used for overnight incubation. After extensive washing with Tris-buffered saline (pH 7.4) and 0.05% Tween 20, the membranes were incubated for 45 minutes with anti-rabbit HRP-coupled secondary antibodies (Jackson Immuno Research, West Grove, PA). The chemiluminescence reaction for horseradish peroxidase (HRP) was developed using self-made chemiluminescence reagent (100 mM Tris pH 8.0, 1.25 mM luminol, 0.2 mM coumaric acid, 0.006% hydrogen peroxide) and visualized with Stella 8300 bio-imager (Raytest, Straubenhardt, Germany). The blots were stripped in 0.1 M glycine (pH 2.6) and reprobed with anti-actin-HRP conjugated rabbit polyclonal antibody (Sigma) at 1:50,000 dilution for 45 minutes. Densitometric analysis was performed using ImageQuant 5.2 software (Amersham Bioscience, Piscataway, NJ).

Real-time Polymerase Chain Reaction

A total of 1×10^6 cells were washed twice with PBS, pelleted, and treated with 1 ml of TRIzol reagent (Invitrogen) to extract total RNA according to the manufacturer's protocol. RNA concentration was measured with Bio-Rad spectrophotometer. The first-strand complementary DNA synthesis containing 100 ng of total RNA was primed with oligo(dT) using Native AMV Reverse Transcriptase (EurX, Gdansk, Poland). The primers for *GLUT1*, *GLUT2*, *GLUT3*, *GLUT4*, and β_2 -microglobulin (*B2M*, reference gene) were custom designed (Table 1). Quantitative real-time polymerase chain reaction (RT-PCR) amplification reactions were performed in the LightCycler II 480 Real-time PCR System (Roche, Mannheim, Germany), using

Table 1. Primers Used for Quantitative RT-PCR.

GLUT1 – (SLC2A1) – NM_006516	CTTTGTGGCCTTCTTTGAAGT	CCACACAGTTGCTCCACAT
GLUT2 – (SLC2A2) – NM_000340.1	AGCTGCATTCAGCAATTGGACC	ATGTGAACAGGGTAAAGGCCAGG
GLUT3 – (SLC2A3) – NM_006931.2	GACAGCCCATCATCATTTCC	TTGAACACCTGCATCCCTTGA
GLUT4 – (SLC2A4) – NM_001042.2	CTTCCAACAGATAGGCTCCG	CCCCAATGTTGTACCCAAAC
β_2 -Microglobulin	TAGGAGGGCTGGCAACTAG	CCAAGATGTTGATGTTGGATA

the LightCycler FastStart DNA Master SYBR Green I Kit (Roche). Data were analyzed using the LightCycler 480 Software 1.5 (Roche). The fold change for each gene relative to the reference gene (*B2M*) was calculated using user-noninfluent, second-derivative method. The specificity of all the reactions was confirmed through analysis of the PCR product's melting profile, obtained by dissociation of the DNA present after the amplification step. The primers and reaction parameters were validated and optimized according to the MIQE (minimum information for publication of quantitative real-time PCR experiments) guidelines. In addition, reaction specificity was also confirmed by agarose gel electrophoresis in which the PCR products were of expected size.

Generation of Raji and HEK293T Cells Stably Expressing HA-GLUT1

A pCIS2 vector expressing human *GLUT1* gene with an HA tag built into the first extracellular loop (hereafter called *HA-GLUT1*) was a generous gift from Dr Samuel W. Cushman from the National Institutes of Health, Baltimore, MD. The *HA-GLUT1* gene was cloned into the pLVX-IRES-Puro vector (Clontech Laboratories, Inc, Mountain View, CA) enabling its lentiviral expression. Next, HEK293T cells were cotransfected with pLVX-HA-GLUT1-IRES-Puro, envelope (pMD2.G), and packaging (pPAX2) vectors using GeneJuice reagent (Calbiochem, San Diego, CA) as a DNA carrier. pMD2.G and pPAX2 plasmids were obtained from Prof Didier Trono (École polytechnique fédérale de Lausanne, Switzerland). Lentivirus-containing supernatants were collected 72 hours after transfection and added to the culture of Raji or HEK293T cells. Positive clones were selected with puromycin (Sigma) and evaluated with flow cytometry using anti-HA-PE antibodies as described previously.

Total Cellular Cholesterol Measurements

Cholesterol concentration was quantified in the Amplex Red cholesterol assay (Invitrogen) in whole-cell Raji lysates. Briefly, samples containing 2.5×10^5 cells were diluted in reaction buffer composed of 300 μ M Amplex Red, 2 U/ml cholesterol oxidase, 2 U/ml cholesterol esterase, and 2 U/ml HRP. The samples were incubated at 37°C for 30 minutes in the dark, and fluorescence was measured at Agilent Bioanalyzer (Agilent Technologies, Santa Clara, CA) equipped with 560-nm excitation and 590-nm emission filters. Cholesterol values were calculated according to the cholesterol standard curve and normalized to the protein content as measured with Bio-Rad Protein Assay (Bio-Rad).

G-actin to F-actin Evaluation

Determination of depolymerized (free globular—G) to polymerized (filamentous—F) actin was performed using a G-actin/F-actin *in vivo* assay kit (Cytoskeleton, Denver, CO) according to the manufacturer's protocol. Briefly, 5×10^5 cells were lysed in F-actin stabilization buffer supplemented with Complete protease inhibitor cocktail (Roche Diagnostics). Next, G-fraction was separated from F-fraction with ultracentrifugation (100,000g for 1 hour at 37°C; Beckman Coulter). Supernatants (G-actin) and pellets (F-actin) were separated electrophoretically in 10% SDS-PAGE gel, blotted onto nitrocellulose membrane (Schleicher & Schuell BioScience), blocked with Tris-buffered saline (pH 7.4) and 0.05% Tween 20, and supplemented with 5% nonfat milk. For β -actin detection, HRP-coupled rabbit polyclonal antibody (Sigma) was used at 1:100,000 dilution for 1 hour of incubation at

room temperature. The reaction was developed with homemade chemiluminescence reagent solution (100 mM Tris pH 8.0, 0.2 mM coumaric acid, 1.25 mM luminol [from Sigma-Aldrich], and 0.006% H_2O_2) using Stella bioimager (Raytest).

Membrane Protein Biotinylation

Control- and drug-treated cells (1×10^7 per each experimental group) washed twice with ice-cold PBS were surface-labeled with 2 mM disulfide-cleavable biotin (EZ-link sulfo-*N*-hydroxysuccinimido [NHS]–biotin [Thermo Scientific, Rockford, IL]) dissolved in biotinylation buffer (10 mM triethanolamine, 2 mM $CaCl_2$, 150 mM NaCl, pH 7.5) for 30 minutes with gentle agitation on ice. The cells were next washed twice in PBS with 100 mM glycine followed by two washes with PBS only and lysed in lysis buffer (10% glycerol, 1.0% Triton X-100, 150 mM NaCl, 5 mM EDTA, 50 mM HEPES, pH 7.4) enriched with protease inhibitors cocktail Complete protease inhibitor cocktail (Roche Diagnostics). Next, samples containing equal amounts of total cellular proteins (300 μ g) were incubated overnight at 4°C on a rotary wheel with 100 μ l of immobilized NeutrAvidin agarose resin (Thermo Scientific)—50% slurry of—to separate the biotinylated surface proteins from nonbiotinylated intracellular proteins. Next, neutravidin-coated agarose beads were spun at 400g for 4 minutes, and the supernatant (nonbiotinylated fraction) was collected and used subsequently as a control of protein loading. The beads were washed thrice in a beads wash buffer (20 mM HEPES, pH 7.4, 150 mM NaCl, 10% glycerol, 0.1% Triton X-100) and boiled in Laemmli sample buffer for 10 minutes at 95°C with gentle shaking that releases biotinylated proteins from their binding with neutravidin. Membrane (biotinylated) and cytosolic proteins were subsequently analyzed with Western blot using anti-GLUT1 (1:1000 dilution; Millipore), anti-intercellular adhesion molecule 1 (ICAM, 1:1000 dilution, Santa Cruz Biotechnology, Santa Cruz, CA) or anti-actin HRP-conjugated (1:50,000 dilution; Sigma) antibodies as described in the Western Blot Analysis section.

Cholesterol Measurements

Total cholesterol concentration in serum of hypercholesterolemic patients on days 0, 3, and 21 of atorvastatin treatment was estimated using a standard cholesterol oxidase method with Cobas Integra 800 analyzer (Roche). Approval for the study was obtained from the institutional review board of the Medical University of Warsaw and was conducted according to the Declaration of Helsinki. Each patient signed a written informed consent for the procedures.

Leukocyte Isolation from Blood

Peripheral blood sample (5 ml) of patients was collected before (day 0), on the third day (day 3), or after 3 weeks (day 21) of atorvastatin (20 mg/day) treatment. The blood was diluted twice with PBS. Next, 3 ml of Histopaque-1077 (Sigma-Aldrich) was pipetted into conical centrifuge tubes. Ten milliliters of diluted peripheral blood was slowly layered on the top of Histopaque layer. Next, tubes were centrifuged (400g for 30 minutes at 21°C) without brake. The buffy coats were isolated and washed twice with PBS. The leukocyte pellet was resuspended in 3 ml of PBS and counted in a Brükler chamber using Türk dye. Peripheral blood leukocytes were used to determine 2-DOG uptake according to the protocol described in the Radioisotope measurement of glucose uptake section of the Materials and Methods. Approval for the study was obtained from the institutional review board of the Medical University of Warsaw and was

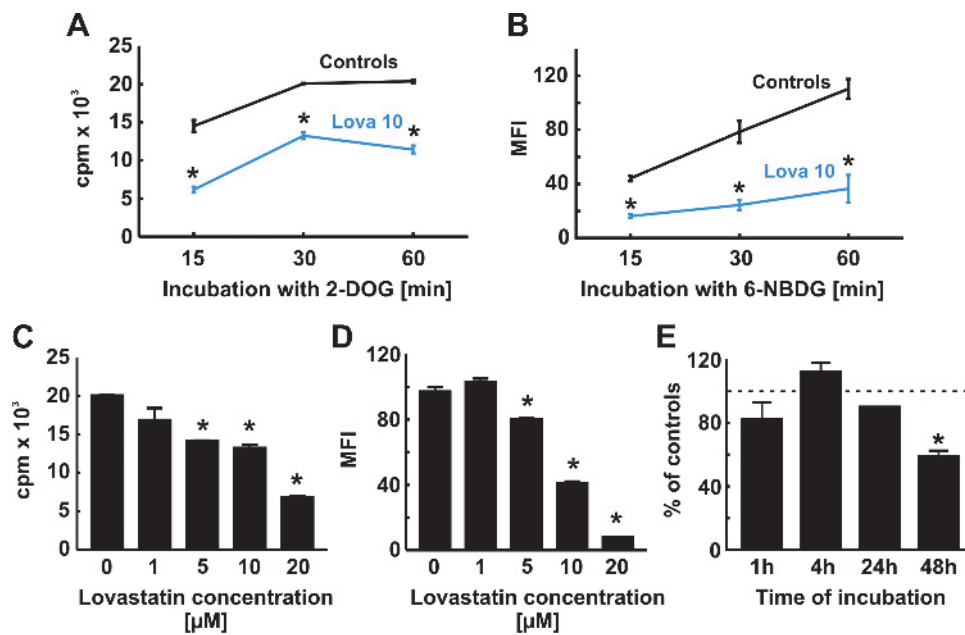


Figure 1. Lovastatin decreases glucose uptake in Raji cells in a time- and dose-dependent fashion. (A) Human Burkitt lymphoma Raji cells were incubated for 48 hours with 10 μM lovastatin. Next, 3×10^5 cells resuspended in 300 μl of transport solution were incubated for 15, 30, or 60 minutes with 1.5 μl of 2-DOG (8.0 mCi/ml radionuclide concentration), and after a three-time wash in cold PBS, the cells were lysed and analyzed in a scintillation counter. The figure presents mean counts per minute (cpm) value \pm SD. $*P < .05$ versus controls in Student's *t* test. (B) Raji cells were incubated for 48 hours with 10 μM lovastatin. Next, 3×10^5 cells were stained for 15, 30, or 60 minutes with 300 μM 6-NBDG in PBS, and after a three-time wash in cold PBS, the cells were analyzed with flow cytometry. The figure presents MFI \pm SD after background subtraction (MFI of Raji cells preincubated for 15 minutes with 200 mM 4,6-ETDG that serves as an extracellular GLUT1 inhibitor). $*P < .05$ versus controls in Student's *t* test. (C) Raji cells were incubated for 48 hours with the indicated lovastatin concentrations. Next, 3×10^5 cells were incubated for 30 minutes with 2-DOG, and after a three-time wash in cold PBS, the cells were lysed and analyzed in a scintillation counter. The figure presents mean cpm \pm SD. $*P < .05$ versus controls in Student's *t* test. (D) Raji cells were incubated for 48 hours with the indicated lovastatin concentrations. Next, 3×10^5 cells were stained for 30 minutes with 300 μM 6-NBDG in PBS, and after a three-time wash in cold PBS, the cells were analyzed by flow cytometry. The figure presents MFI \pm SD after background subtraction. $*P < .05$ versus controls in Student's *t* test. (E) Raji cells were incubated for indicated time with 10 μM lovastatin. Next, 3×10^5 cells were incubated for 30 minutes with 2-DOG, and after a three-time wash in cold PBS, the cells were lysed and analyzed in a scintillation counter. The figure presents mean cpm \pm SD as a percentage of controls. $*P < .05$ versus controls in Student's *t* test.

conducted according to the Declaration of Helsinki. Each patient gave a written informed consent for the procedures.

Positron Emission Tomography/Computed Tomography

Whole-body PET/CT examinations in three-dimensional mode (2 minutes per bed position) were performed on PET/CT scanner Biograph 64 TruePoint (Siemens Medical Solutions, Erlangen, Germany). The PET studies were performed 55 to 65 minutes after injection of 350 to 360 MBq ^{18}F -FDG. All patients were requested to drink 1.5 L of water-equivalent oral contrast dispersion. Immediately before the PET/CT examination, patients were requested to empty their bladder. Patients were positioned head first supine on the common patient handling system with the arms raised in according with standard CT practice. Coaxial whole-body imaging ranges were defined on the Topogram, covering the area from the skull to the upper thighs (2 minutes, six to seven PET bed positions depending on the size of the patient—one PET bed have approximately 15 cm). CT was performed in spiral mode using a continuous acquisition at 120 kV, 170 mA, 2-mm slice width, and pitch of 0.8. Emission data were reconstructed with attenuation correction based on low-dose CT. PET emission data were reconstructed (reconstruction method—TrueX) using an attenuation-weighted approach on 168 \times 168 matrices and with a 4-mm Gaussian postrecon-

struction filtering (two iterations, 14 subsets). The PET/CT images were assessed using Multimodality Work Station Syngo (TrueD) by Siemens. All pathologic foci of ^{18}F -FDG uptake were included in the evaluation. Uptake in organs was evaluated assuming a uniform distribution in the organ of interest. Regions of interest (ROIs) were drawn around each foci. Maximum standardized uptake values (SUV_{max}) were calculated in all ROIs. CT data were used for allocation of regions with increased uptake of the radiopharmaceutical to specific morphologic structures. The study was approved by the ethical

Table 2. Changes in Lactate Concentration Correlate with Impaired Glucose Uptake in Raji Cells.

Group	Lactate Concentration in Medium (Mean μmol of Lactate/ μg of Total Cellular Protein \pm SD)	6-NBDG Uptake (Mean Fluorescence Intensity \pm SD)	% of PI-Positive Cells (Mean \pm SD)
Controls	0.215 \pm 0.005	79.21 \pm 4.75	10.03 \pm 0.28
10 μM lovastatin for 24 h	0.116 \pm 0.005*	63.90 \pm 0.07*	14.10 \pm 6.5
10 μM lovastatin for 48 h	0.091 \pm 0.002*	30.75 \pm 2.40*	14.85 \pm 0.54

* $P < .05$ versus controls (Student's *t* test).

committee of Medical University of Warsaw. All patients have given an informed consent.

Results

Lovastatin Inhibits Glucose Uptake

To investigate the influence of cholesterol synthesis, inhibitors on the glucose uptake Raji cells were preincubated with 10 μM lovastatin for 48 hours and, after washing with PBS, were incubated with either tritiated 2-DOG or 6-NBDG. Glucose uptake was measured after 15, 30, or 60 minutes of incubation after extensive washing of cells with PBS using scintillation counter or flow cytometry. The results of these experiments revealed that the glucose uptake was strongly suppressed in lovastatin-pretreated cells compared with controls with a maximum of almost three-fold decrease in uptake observed for 2-DOG at 15 minutes and for 6-NBDG at 60 minutes (Figure 1, A and B). Lovastatin-mediated inhibition of glucose uptake was concentration dependent, observed already at 5 μM lovastatin concentration for both 2-DOG and 6-NBDG (Figure 1, C and D). The inhibition of glucose uptake was unlikely to result from unspecific binding of lovastatin to GLUTs that could lead to inhibition of their activity because it occurred after at least a 48-hour incubation (Figure 1E). Inhibition of glucose uptake correlated with

decreased lactate production in cells incubated with 10 μM lovastatin for 24 and 48 hours (Table 2). Lovastatin-mediated inhibition of glucose uptake was also observed in other cell lines including Daudi, Ramos, DoHH2 lymphomas, LoVo colon adenocarcinoma, as well as HEK293T cells (Figure 2A). It was previously shown that glucose uptake can be dependent on the rate of tumor cells' proliferation [23,24]. However, at studied concentrations, lovastatin did not significantly affect the cell cycle of Raji cells. In controls, 51% of cells were in the G₁ phase, 26% were in the S phase, and 23% were in the G₂ phase. In cells incubated with 10 or 20 μM lovastatin, the values were 60% and 63% for the G₁ phase, 19% and 20% for the S phase, and 21% and 17% for the G₂ phase, respectively (Figure 2B). Analysis of cytostatic/cytotoxic effects measured using 3-(4,5-dimethylthiazol-2-yl)-2,5-diphenyltetrazolium bromide assay has also demonstrated that lovastatin is not toxic at the concentrations studied (data not shown). Other statins, including cerivastatin, simvastatin, fluvastatin, and atorvastatin (all except 1 μM cerivastatin were used at 10 μM concentrations), have also significantly impaired 6-NBDG uptake by Raji cells (Figure 2C).

Lovastatin Does Not Impair Expression of GLUT Genes

Statins can modulate expression of many different genes. Quantitative RT-PCR was used to determine the influence of lovastatin on the expression of GLUT genes, including *GLUT1*, *GLUT2*,

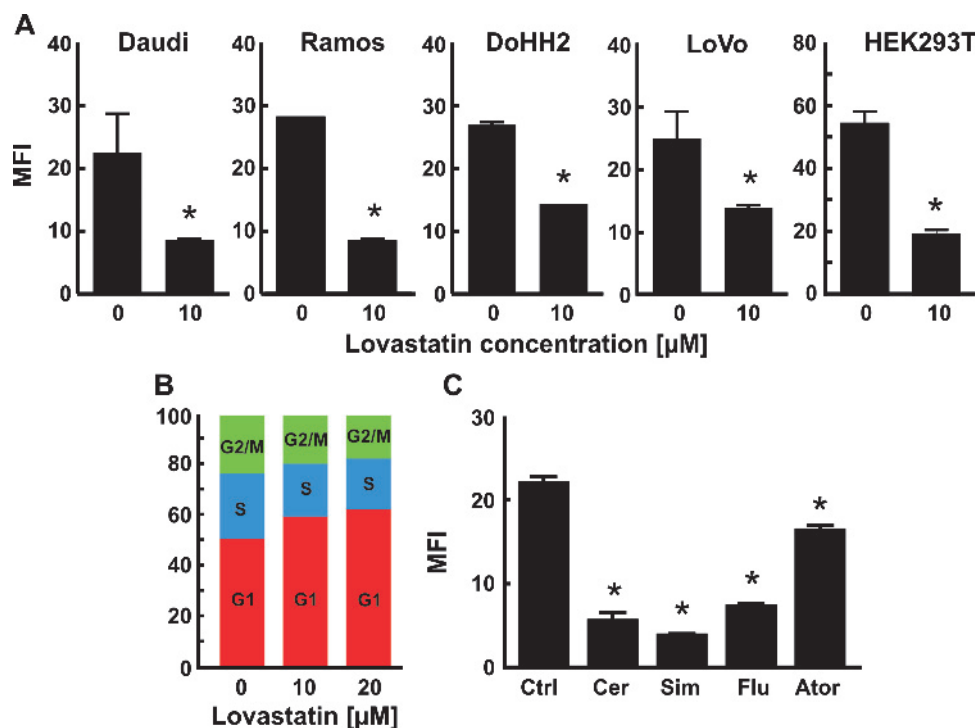


Figure 2. Statins decrease glucose uptake in human malignant and nonmalignant cell lines. (A) Human Burkitt lymphoma (Daudi, Ramos), follicular B-cell lymphoma (DoHH2), colon adenocarcinoma (LoVo), and embryonic kidney (HEK293T) cells were incubated for 48 hours with 10 μM lovastatin. Next, 3×10^5 cells were stained for 30 minutes with 300 μM 6-NBDG in PBS and after a three-time wash in cold PBS, the cells were analyzed with flow cytometry. The figure presents MFI \pm SD after background subtraction. * $P < .05$ versus controls in Student's *t* test. (B) Raji cells were incubated for 48 hours with 10 or 20 μM lovastatin. Next, 5×10^5 cells were fixed for 1 hour in ice-cold 70% ethanol, washed, stained with 5 $\mu\text{g}/\text{ml}$ of propidium iodide, and analyzed with flow cytometry. The figure presents the percentage distribution of cells in the G₁, S, and G₂/M cell cycle phase. (C) Raji cells were incubated for 48 hours with 1 μM cerivastatin (Cer), 10 μM simvastatin (Sim), 10 μM fluvastatin (Flu), and 10 μM atorvastatin (Ator). Next, 3×10^5 cells were stained for 30 minutes with 300 μM 6-NBDG in PBS, and after a three-time wash in cold PBS, the cells were analyzed with flow cytometry. The figure presents MFI \pm SD after background subtraction. * $P < .05$ versus controls in Student's *t* test.

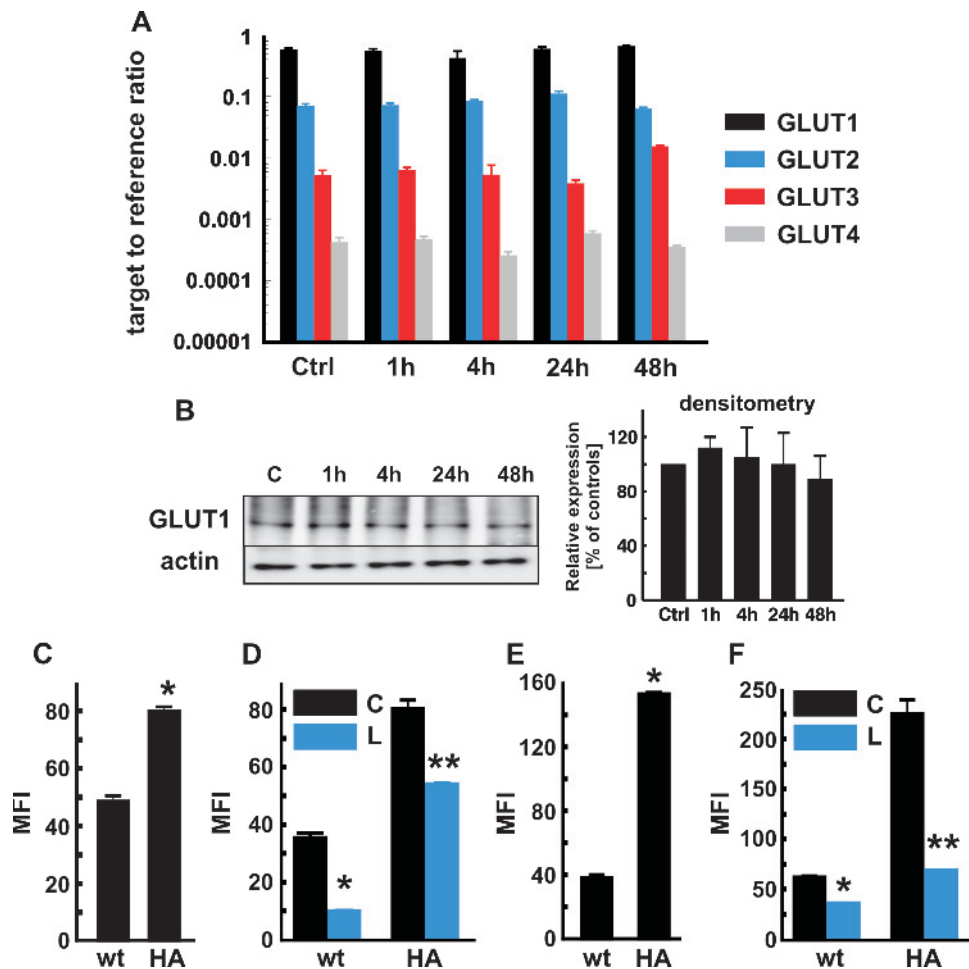


Figure 3. Lovastatin does not influence overall expression of GLUT 1, 2, 3, and 4 but impairs glucose uptake in HA-GLUT1 overexpressing cells. (A) Raji cells were incubated for indicated time with 10 μ M lovastatin. Next, the expression of *GLUT1*, *GLUT2*, *GLUT3*, and *GLUT4* was evaluated in quantitative RT-PCR. The figure presents mean target-to-reference ratio \pm SD. (B) Raji cells incubated for 1 hour to 48 hours with 10 μ M lovastatin were lysed, and total GLUT1 protein levels were analyzed with Western blot analysis. Actin served as a loading control. The figure shows the representative result. The obtained data were semiquantified with densitometry. (C) 6-NBDG uptake by wild-type (wt) and HA-GLUT1-expressing (HA-GLUT1) Raji cells. A total of 3×10^5 cells were stained for 30 minutes with 300 μ M 6-NBDG in PBS, and after a three-time wash in cold PBS, the cells were analyzed with flow cytometry. The figure presents MFI \pm SD after background subtraction. * $P < .05$ versus wt cells in Student's *t* test. (D) Nontransduced (wt) and HA-GLUT1-expressing Raji cells (HA-GLUT1) were incubated for 48 hours with 10 μ M lovastatin. Next, 3×10^5 cells were stained for 30 minutes with 300 μ M 6-NBDG in PBS, and after a three-time wash in cold PBS, the cells were analyzed with flow cytometry. The figure presents MFI \pm SD after background subtraction. * $P < .05$ versus control wt group in Student's *t* test. ** $P < .05$ versus control HA-GLUT1 group in Student's *t* test. "C" stands for control (=no lovastatin-treated) group of each cell line; "L" stands for lovastatin-treated group. (E) 6-NBDG uptake by wild-type (wt) and HA-GLUT1-expressing (HA-GLUT1) HEK293T cells. A total of 3×10^5 cells were stained for 30 minutes with 300 μ M 6-NBDG in PBS, and after a three-time wash in cold PBS, the cells were analyzed with flow cytometry. The figure presents MFI \pm SD after background subtraction. * $P < .05$ versus wt cells in Student's *t* test. (F) Nontransduced (wt) and HA-GLUT1-expressing HEK293T cells (HA-GLUT1) were incubated for 48 hours with 5 μ M lovastatin. Next, 3×10^5 cells were stained for 30 minutes with 300 μ M 6-NBDG in PBS, and after a three-time wash in cold PBS, the cells were analyzed with flow cytometry. The figure presents MFI \pm SD after background subtraction. * $P < .05$ versus control wt group in Student's *t* test. ** $P < .05$ versus control HA-GLUT1 group in Student's *t* test. "C" stands for control (=no lovastatin-treated) group of each cell line; "L" stands for lovastatin-treated group.

GLUT3, and *GLUT4* in Raji cells. The expression of investigated GLUTs did not change in cells incubated with 10 μ M lovastatin (Figure 3A). Also, at the protein level, the amount of GLUT1 did not change in lovastatin-treated Raji cells compared with controls (Figure 3B). Determination of other GLUT proteins was not possible owing to the poor quality of available antibodies.

To address the potential influence of statins on the transcriptional regulation of glucose transport in more detail, Raji cells were stably

transduced with lentiviral vector encoding HA-tagged GLUT1 under constitutive CMV promoter. Glucose uptake by HA-GLUT1-transduced Raji and HEK cells was significantly higher as compared with controls (Figure 3, C and E). However, incubation of control and HA-GLUT1-transduced Raji and HEK cells with 10 μ M lovastatin for 48 hours resulted in significant inhibition of glucose uptake (Figure 3, D and F), indicating that it is the activity and not the expression level of GLUT1 that is suppressed in lovastatin-treated cells.

GLUT4 undergoes cycling from the plasma membrane through an actin-dependent fast endocytosis and slow exocytosis that can be accelerated by insulin [25]. In contrast, GLUT1 is an insulin-independent, constitutive transporter, and there is no strong evidence indicating its cycling between membrane and endosomal compartments. To investigate the possibility that statins might interfere with GLUT cycling, the influence of statins on the organization of actin fibers was investigated. Phalloidin and cytochalasin D were used as positive controls to either promote or disrupt actin polymerization, respectively (Figure 4A). However, neither lovastatin nor atorvastatin was able to influence the organization of actin fibers in Raji cells (Figure 4B). Additional experiments with biotinylation of extracellular proteins followed by immunoprecipitation revealed that the levels of GLUT1 in intracellular as well as membrane compartments remain comparable in control and lovastatin-treated cells (Figure 4C). These results indicate that lovastatin does not affect trafficking of GLUT1 proteins in Raji cells.

Impaired Glucose Uptake Results from Inhibition of Cholesterol Synthesis

Incubation of Raji cells with lovastatin decreased total cholesterol content by 15% (Table 3). Considering that cholesterol concentra-

Table 3. Changes in Cellular Cholesterol Concentration on Incubation with Lovastatin.

Group	Amount of Cholesterol in 2.5×10^5 Cells (Mean \pm SD; ng)
Controls	2.89 \pm 0.02
10 μ M lovastatin for 48 h	2.46 \pm 0.09*
10 μ M lovastatin + 200 μ M MA for 48 h	2.71 \pm 0.04†

* $P < .05$ versus controls (Student's t test).

† $P < .05$ versus lovastatin-treated group (Student's t test).

tion is tightly regulated in mammalian cells, this 15% drop is highly relevant. Cholesterol depletion can be achieved using M β CD, which acutely extracts cholesterol from the exoplasmic leaflet of the plasma membrane [26]. A 30-minute incubation of Raji cells with 5 mg/ml of M β CD resulted in almost four-fold inhibition of 6-NBDG uptake (Figure 5A), indicating the possibility that statin-mediated impairment of intracellular glucose transport might result from diminished plasma membrane cholesterol content. Statin-mediated inhibition of cholesterol synthesis can be restored by exogenous MA or FPP [27]. Coincubation of Raji cells with 10 μ M lovastatin and 10 μ M FPP or 200 μ M MA resulted in restoration of glucose uptake in Raji cells (Figure 5B). Moreover, L-744,832, a farnesyltransferase inhibitor, increased rather than decreased glucose uptake by Raji cells, indicating that impaired statin-mediated glucose transport is unlikely to be caused by interference with protein prenylation (Figure 5C). Repletion of cellular cholesterol with cholesterol-M β CD complexes restored glucose uptake in lovastatin-treated cells (Figure 5, D and E).

Influence of Atorvastatin on Glucose Uptake by Peripheral Blood Mononuclear Cell in Patients

A small exploratory clinical study was performed to investigate the influence of cholesterol depletion in freshly isolated peripheral blood mononuclear cells (PBMCs) from patients diagnosed with hypercholesterolemia who were treated with atorvastatin. Eight patients were treated for 3 weeks with a daily dose of 20 mg atorvastatin to reduce their cholesterol blood concentration and to determine the glucose uptake in freshly isolated PBMCs. Peripheral blood was collected on days 0 (before administration of atorvastatin), 3, and 21 to measure plasma cholesterol concentration and 2-DOG uptake. In three patients (patients 1, 2, and 4 in Figure 6), there was a correlation between decreased plasma cholesterol concentration and 2-DOG uptake, although in patient 4, there was an initial drop in cholesterol concentration accompanied by a decrease in 2-DOG uptake, followed by a rise in both parameters on day 21. In the remaining patients, despite a slightly decreased cholesterol concentration on day 3, there was an increase in 2-DOG uptake, but after 3 weeks, a decreased cholesterol concentration was accompanied by a drop in 2-DOG uptake. A higher variability of results obtained in a heterogeneous population of patients compared with cell culture models, where all experimental conditions are well controlled, might result from several factors. For example, differences in nutritional habits, stress level, sport activity, and others might all affect the final results obtained in the pilot study. Also, genetic polymorphisms in various metabolic pathways can be expected to play a role. At least to some extent, the variability might also result from the patients' incomplete adherence to the prescribed atorvastatin.

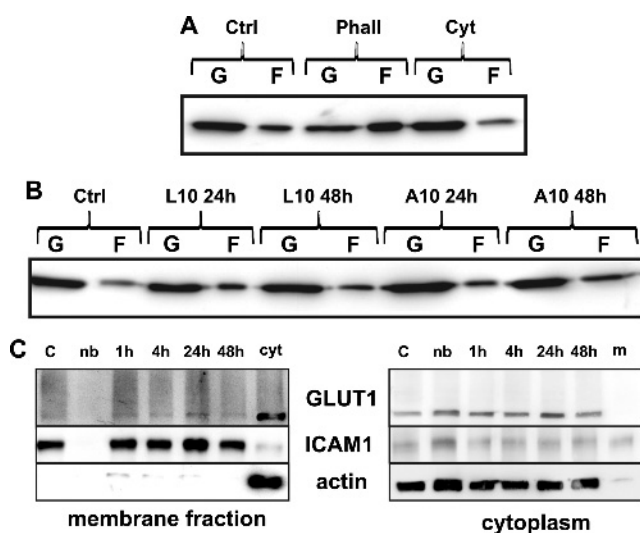


Figure 4. Statins do not influence actin fibers' organization as well as membrane GLUT1 protein expression in Raji cells. (A) Control experiment—Raji cell lysates were incubated for 5 minutes with 1 μ M phalloidin (Phall) or 10 μ M cytochalasin D (Cyt). After ultracentrifugation, F (fibrillar) and G (globular) fractions were evaluated in Western blot analysis. (B) Raji cells were incubated for 24 or 48 hours with 10 μ M lovastatin (L) or atorvastatin (A). Next, F (fibrillar) and G (globular) fractions in cell lysates were evaluated in Western blot analysis using G-actin/F-actin *in vivo* assay kit from Cytoskeleton. (C) Membrane proteins of Raji cells incubated for 1 hour to 48 hours with 10 μ M lovastatin were labeled with cell-nonpermeable NHS biotin. Next, the cells were lysed, and biotin-bound membrane proteins were precipitated with neutravidin beads. The figure presents Western blot results of membrane and cytosolic protein fractions for GLUT1, ICAM1 (membrane protein control), and actin (cytosolic protein control). cyt (cytosolic fraction) and m (membrane fraction) served as controls for subsequent antibody reactivity. nb indicates nonbiotinylated group.

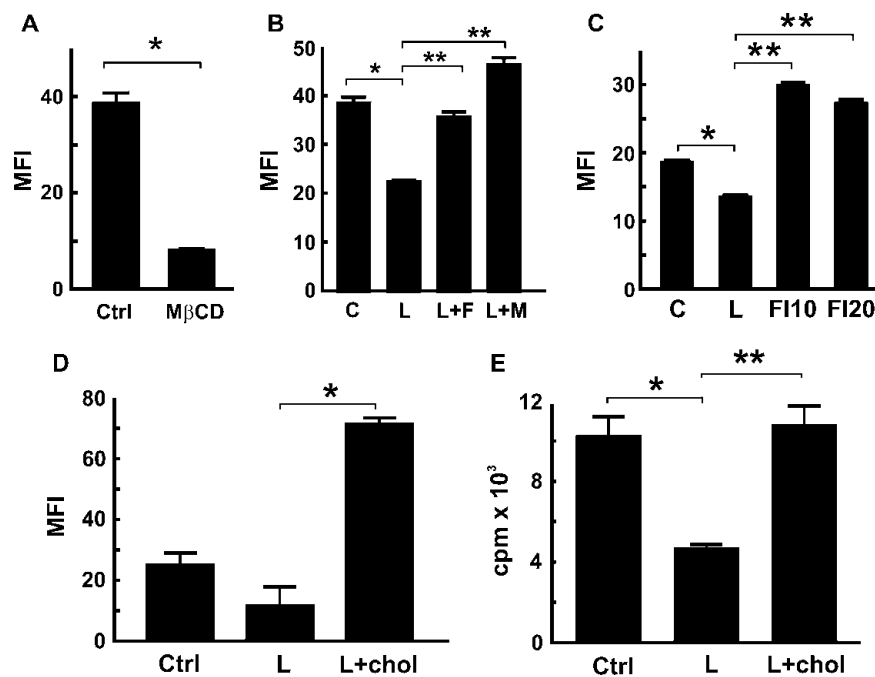


Figure 5. Effects of lovastatin on glucose uptake depend on the cholesterol biosynthesis pathway. (A) Raji cells were incubated for 30 minutes with 5 mg/ml MβCD. Next, 3×10^5 cells were stained for 30 minutes with 300 μM 6-NBDG in PBS, and after a three-time wash in cold PBS, the cells were analyzed with flow cytometry. The figure presents MFI ± SD after background subtraction. * $P < .05$ versus controls in Student's t test. (B) Raji cells were incubated for 48 hours with 10 μM lovastatin (L), 10 μM FPP (F), and/or 200 μM MA (M). Next, 3×10^5 cells were stained for 30 minutes with 300 μM 6-NBDG in PBS, and after a three-time wash in cold PBS, the cells were analyzed with flow cytometry. The figure presents MFI ± SD after background subtraction. * $P < .05$ versus controls in Student's t test. ** $P < .05$ versus lovastatin-treated group in Student's t test. (C) Raji cells were incubated for 48 hours with 10 μM lovastatin (L) and 10 μM or 20 μM farnesyltransferase inhibitor L-744,832 (FI). Next, 3×10^5 cells were stained for 30 minutes with 300 μM 6-NBDG in PBS, and after a three-time wash in cold PBS, the cells were analyzed with flow cytometry. The figure presents MFI ± SD after background subtraction as a percentage of controls. * $P < .05$ versus controls in Student's t test. (D) Raji cells were incubated for 48 hours with 10 μM lovastatin (L). For the last 30 minutes of incubation, 0.2 mg/ml of water-soluble cholesterol-MβCD (chol) was added. Next, 3×10^5 cells were stained for 30 minutes with 300 μM 6-NBDG in PBS, and after a three-time wash in cold PBS, the cells were analyzed with flow cytometry. The figure presents MFI ± SD after background subtraction. * $P < .05$ versus lovastatin-treated group in Student's t test. (E) Raji cells were incubated for 48 hours with 10 μM lovastatin (L). For the last 30 minutes of incubation, 0.2 mg/ml of water-soluble cholesterol-MβCD (chol) was added. Next, 3×10^5 cells were incubated for 30 minutes with 2-DOG, and after a three-time wash in cold PBS, the cells were lysed and analyzed in a scintillation counter. The figure presents mean cpm ± SD. * $P < .05$ versus lovastatin-treated group in Student's t test.

Influence of Atorvastatin on ¹⁸F-FDG Uptake in Cancer Patients

The influence of statins on glucose uptake might affect the diagnostic procedures using ¹⁸F-FDG PET. To investigate this possibility, PET/CT with ¹⁸F-FDG examinations were performed before and after atorvastatin treatment in four patients (briefly described in Table 4) referred to the Nuclear Medicine Department of Medical University of Warsaw. Second PET/CT imaging was performed within a 1-week period after administration three atorvastatin doses of 40 mg. The imaging parameters (dose and time of acquisition) and protocol on patient preparation were comparable in both examinations. ¹⁸F-FDG uptake was not suppressed in patients 2, 3, and 4. However, a strongly decreased ¹⁸F-FDG uptake was observed in patient 1. In this patient, baseline SUV_{max} levels were 12.8 (range = 12.3-16.7) and 5.95 (range = 5.6-8.9) before and after atorvastatin treatment, respectively (Table 5). A PET/CT scan of thoracic cavity before and after atorvastatin treatment, indicating decreased ¹⁸F-FDG uptake in patient 1, is shown in Figure 7.

Discussion

Statins are among the most frequently prescribed drugs. They exert lipid-lowering effects and are used in the prevention and treatment of cardio-

vascular diseases. Besides lowering plasma cholesterol concentration, statins exert pleiotropic effects that are presumed to be independent of their cholesterol-lowering properties [28,29]. These include improved endothelial function, decreased vascular inflammation, neuroprotection, and many others [29]. Intriguingly, some of these putative pleiotropic effects might be detrimental and responsible for the adverse effects of statin treatment. For example, potential diabetogenic effects of statins have been reported in a randomized trial of rosuvastatin for primary prevention (JUPITER) [30]. Although these observations are at odds with previous primary prevention statin trial (WOSCOPS) [31], a recent collaborative meta-analysis that collected data from 13 large placebo-controlled trials indicate that statin therapy is associated with a slightly increased risk of development of diabetes [32,33]. Also, a lipid-modifying niacin has been reported to increase the risk of developing diabetes [34]. Together with the findings reported here showing statin-mediated modulation of GLUT activity, the clinical observations revealing alterations in glucose metabolism might be specifically related to drug-induced influence on cholesterol levels. This possibility can be strengthened by our preliminary studies, also indicating that statins impair glucose uptake in a number of normal cells of hepatic, adipose, muscle, or endothelial origin (not shown).

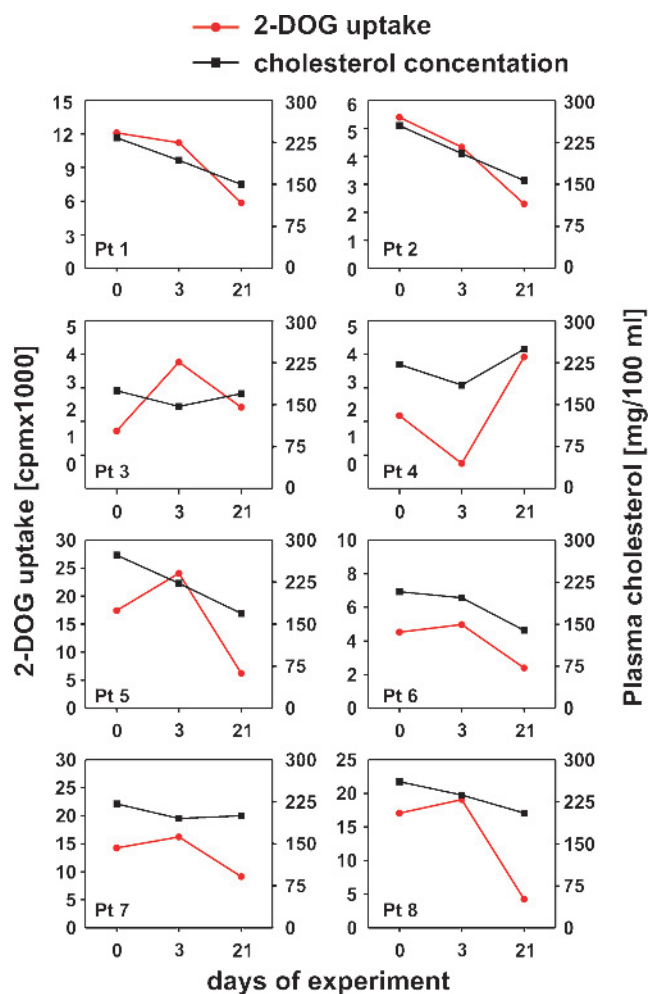


Figure 6. Statins impair glucose uptake in PBMCs. PBMCs were isolated from blood samples collected from patients at days 0, 3, and 21 of atorvastatin treatment (20 mg/d orally). Next, the 2-DOG uptake was evaluated as described in the corresponding Materials and Methods section. The figure presents results of plasma cholesterol levels (right vertical axis) and 2-DOG uptake (left vertical axis) in eight independent patients.

Because HMG-CoA reductase is the rate-limiting enzyme of the mevalonate pathway, potential mechanisms underlying some of these pleiotropic effects include the inhibition of isoprenoid synthesis by statins. Prenyl groups serve as lipid attachments for posttranslational modifications of proteins such as lamins, Ras, Rho, Rap, Rac, and Cdc42 [35]. Isoprenylated proteins constitute up to 2% of all cellular proteins, and their isoprenylation is necessary for correct subcellular localization and function. Other cholesterol-independent effects of statins have also been reported. For example, statins can bind to β_2 -

Table 4. Clinical Data of Four Patients Examined with ^{18}F -FDG PET/CT Imaging Included into the Study.

Patient	Age (years)	Sex	Disease
1	68	M	Mantle cell lymphoma
2	45	F	Follicular lymphoma
3	48	F	Neuroendocrine tumors with unknown primary site
4	18	F	Hodgkin disease

Table 5. ^{18}F -FDG PET/CT Results Obtained in Four Patients before and 3 Days after Initiation of Atorvastatin Treatment.

Patient No.	Focus of Uptake	SUV _{max} before Atorvastatin Treatment	SUV _{max} after Atorvastatin Treatment
1	Cervical lymph node	16.7	8.9
	Supraclavicular lymph node	12.7	5.9
	Paratracheal lymph node	14.4	7.1
	Supracarina lymph node	15.2	6.2
	Axillary lymph node	12.3	5.7
	Para-aortic lymph node	12.6	5.6
2	Iliac lymph node	12.9	5.8
	Inguinal lymph node	12.7	6
	Cervical lymph node	6.7	7.6
	Supramandibular lymph node	8.9	10.4
	Lateral neck lymph node	4.5	4.8
	Para-aortic lymph node	4.1	4.6
3	Liver metastases	14.2	16.6
		12.8	16.9
		9.4	11.7
		8.5	11.2
		7.9	13.6
		7.8	12.4
4	Anterior mediastinum mass	8.4	7.3
	Mediastinum lymph node	5.3	5.3

integrin leukocyte function-associated antigen 1, thereby impairing its function, independently of their influence on the mevalonate pathway [36]. Statins can also affect glycosylation of cellular proteins by inhibiting the mevalonate pathway-derived dolichols and might negatively affect muscle function owing to the inhibition of ubiquinone (coenzyme Q10) production [37,38]. Accumulating evidence indicates that statins can also exert certain effects independently of lowered plasma cholesterol levels, but still resulting from diminished cholesterol synthesis in cells. For example, statins might affect composition and structure of lipid rafts thereby modulating multiple signaling pathways [39,40]. Moreover, we have previously shown that statins can induce conformational changes within CD20 tetraspanin that were reversed by the addition of exogenous cholesterol [13]. Membrane cholesterol levels are strictly controlled and multiple complex mechanisms are evolved, which maintain its homeostasis within a narrow range [41]. Cholesterol is thought to rigidify the fluid plasma membrane to reduce passive permeability and increase its mechanical properties [42]. However, the role of this lipid seems to be more complex. Cholesterol can associate with a number of membrane proteins, either covalently or through noncovalent interactions. Moreover, cholesterol allows condensation of membrane lipids, thus decreasing the area per molecule [43]. Because plasma membrane behaves as an incompressible fluid, the addition of cholesterol increases its total thickness and allows its reorganization. This has significant consequences for the functioning of membrane-embedded proteins [43].

GLUT1 is among the most intensively studied transmembrane proteins; despite this, little is known about the mechanism of glucose transport [44]. It seems that glucose transport occurs through substrate binding-induced conformational change in GLUT1 that leads to substrate translocation [45]. GLUT proteins are extremely difficult to crystallize [44]. Moreover, obtaining crystal structures of membrane-embedded proteins poses additional technical difficulties [46] and only a few proteins have been crystallized in lipid environment [47,48]. Therefore, direct investigation of conformational changes in GLUTs induced by statins will require significant technical advancements.

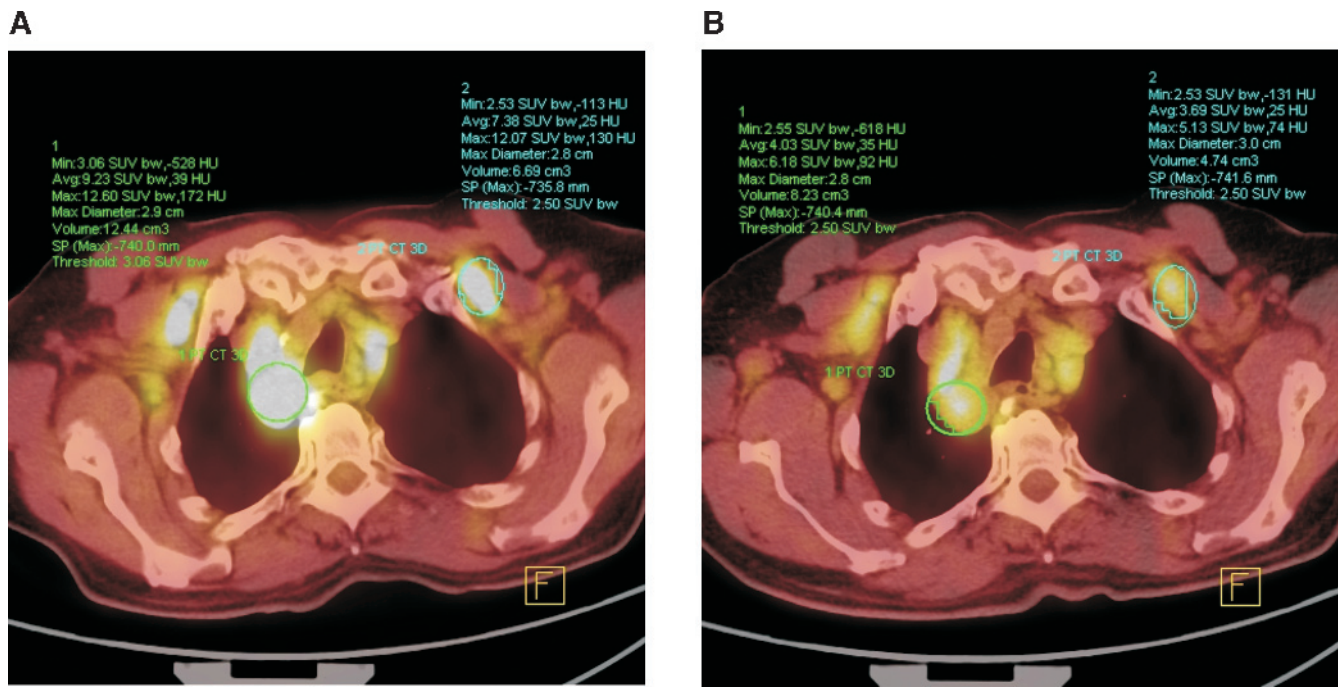


Figure 7. ¹⁸F-FDG PET/CT examination in the patient with mantle cell lymphoma—thoracic scan. (A) Before atorvastatin treatment. (B) Examination of the same anatomic region repeated after three doses of atorvastatin treatment shows a significant decrease in ¹⁸F-FDG uptake in lymph nodes.

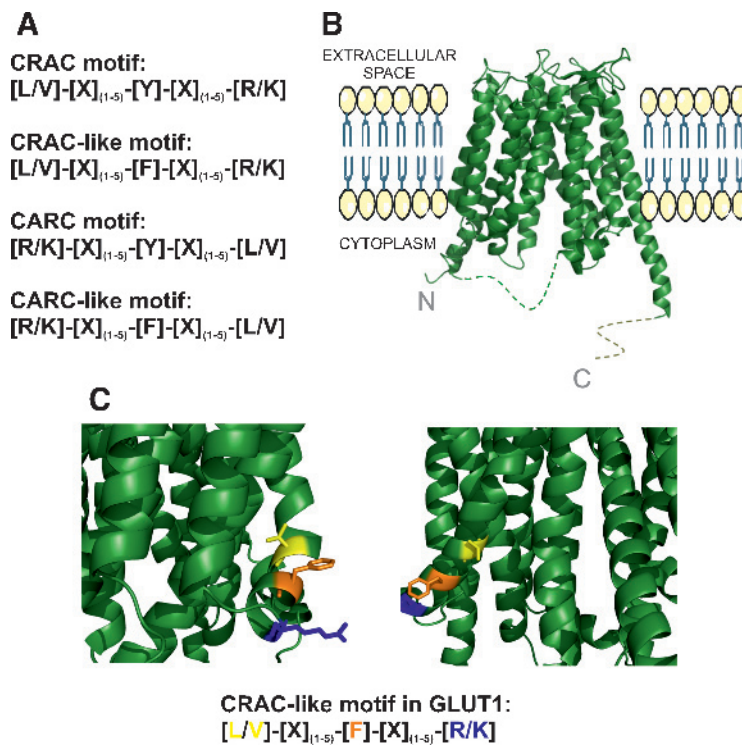


Figure 8. Localization of putative cholesterol-binding motifs in the homology model of human GLUT1 protein. (A) Sequences of cholesterol-binding motifs. (B) A homology model of human GLUT1 protein: N- and C-termini are indicated and the placement within the plasma membrane is only schematic. Disordered/unstructured regions (residues 225-260 and 470-490) are indicated by dashed lines. (C) Putative CRAC-like motifs in GLUT1: aa 83-89 (VGLFVNR, left) and aa 322-330 (VSLFVVER, right).

Proteins that interact with cholesterol contain an amino acid consensus sequences termed *cholesterol recognition/interaction amino acid consensus* (CRAC) or CRAC-like within their juxtamembrane regions [49]. A recent study revealed that acetylcholine receptors contain an inverted CRAC, or CARC motifs within the membrane-embedded regions of the receptor [21]. To identify putative CRAC, CRAC-like, or CARC motifs within GLUT, a bioinformatics analysis was performed. The structure of the human GLUT1 protein was predicted by the comparative modeling approach. First, the GeneSilico metaserver [50] was used to identify the best template for modeling of GLUT1. It identified the structure of the glycerol-3-phosphate transporter from *Escherichia coli* as the most closely related protein to GLUT1 with experimentally determined structure (Protein Data Bank code 1pw4) and provided a series of sequence alignments. Homology modeling was carried out using the “Frankenstein’s monster” approach, in which a protein structure is constructed by iterative model building and splicing fragments from alternative models (see Kosinski et al. [51] for a detailed description of the protocol). This analysis revealed the presence of two CRAC-like cholesterol interaction consensus sequences within a membrane-embedded region of GLUT1 (Figure 8).

Our studies reveal that statins do not inhibit expression of GLUT proteins, and their influence on glucose transport can be reversed by addition of exogenous metabolites of cholesterol biosynthesis pathway (MA or FPP). Moreover, statin-induced effects can be swiftly, that is, within 30 minutes, reversed by coculture of tumor cells with cholesterol-M β CD complexes that restore plasma membrane cholesterol content. Also, M β CD, which extracts cholesterol from plasma membrane is able to induce rapid changes in glucose uptake that would outpace potential influence on the transcriptional regulation of genes encoding GLUTs. These observations indicate that statins are unlikely to impair glucose uptake at transcriptional level. Although statins can also influence posttranscriptional prenylation of multiple proteins, including Rab proteins that regulate endocytosis and exocytosis as well as intracellular trafficking of multiple proteins, there are no data indicating that GLUT1 could be regulated in this manner. Moreover, neither lovastatin nor atorvastatin, at least at the concentrations used, was able to affect the polymerization of actin fibers that might influence the trafficking of GLUT proteins.

Altogether, the results of this study indicate that statins can effectively inhibit glucose uptake by tumor cells. The relevance of this observation might be double-edged. On one hand, statins might interfere with tumor cells’ metabolism, thereby impairing adaptation of tumor cells to microenvironmental conditions associated with tumor progression. It is possible that the reported statin-dependent induction of autophagy in tumor cells [52] results from impaired glucose uptake that triggers autophagy to gain a different source of energy in rapidly proliferating cells. On the other hand, the influence of statins on glucose uptake might be detrimental in diagnostic procedures using ¹⁸F-FDG PET. Our observation should inspire further studies to see if a temporary withdrawal from statin treatment can increase the sensitivity of this diagnostic procedure.

Acknowledgments

The authors thank Anna Czerepinska and Elzbieta Gutowska for their excellent technical assistance.

References

[1] Levine AJ and Puzio-Kuter AM (2010). The control of the metabolic switch in cancers by oncogenes and tumor suppressor genes. *Science* **330**, 1340–1344.

[2] Cairns RA, Harris IS, and Mak TW (2011). Regulation of cancer cell metabolism. *Nat Rev Cancer* **11**, 85–95.

[3] Busk M, Horsman MR, Kristjansen PE, van der Kogel AJ, Bussink J, and Overgaard J (2008). Aerobic glycolysis in cancers: implications for the usability of oxygen-responsive genes and fluorodeoxyglucose-PET as markers of tissue hypoxia. *Int J Cancer* **122**, 2726–2734.

[4] Gillies RJ and Gatenby RA (2007). Adaptive landscapes and emergent phenotypes: why do cancers have high glycolysis? *J Bioenerg Biomembr* **39**, 251–257.

[5] Kurokawa T, Yoshida Y, Kawahara K, Tsuchida T, Okazawa H, Fujibayashi Y, Yonekura Y, and Kotsuji F (2004). Expression of GLUT-1 glucose transfer, cellular proliferation activity and grade of tumor correlate with [F-18]-fluorodeoxyglucose uptake by positron emission tomography in epithelial tumors of the ovary. *Int J Cancer* **109**, 926–932.

[6] Yen TC, See LC, Lai CH, Yah-Huei CW, Ng KK, Ma SY, Lin WJ, Chen JT, Chen WJ, Lai CR, et al. (2004). ¹⁸F-FDG uptake in squamous cell carcinoma of the cervix is correlated with glucose transporter 1 expression. *J Nucl Med* **45**, 22–29.

[7] Higashi T, Tamaki N, Honda T, Torizuka T, Kimura T, Inokuma T, Ohshio G, Hosotani R, Imamura M, and Konishi J (1997). Expression of glucose transporters in human pancreatic tumors compared with increased FDG accumulation in PET study. *J Nucl Med* **38**, 1337–1344.

[8] Augustin R (2010). The protein family of glucose transport facilitators: it’s not only about glucose after all. *IUBMB Life* **62**, 315–333.

[9] Furuta E, Okuda H, Kobayashi A, and Watabe K (2010). Metabolic genes in cancer: their roles in tumor progression and clinical implications. *Biochim Biophys Acta* **1805**, 141–152.

[10] Kaira K, Endo M, Abe M, Nakagawa K, Ohde Y, Okumura T, Takahashi T, Murakami H, Tsuya A, Nakamura Y, et al. (2010). Biologic correlation of 2-[¹⁸F]-fluoro-2-deoxy-D-glucose uptake on positron emission tomography in thymic epithelial tumors. *J Clin Oncol* **28**, 3746–3753.

[11] Bos R, van Der Hoeven JJ, van Der Wall E, van Der Groep P, van Diest PJ, Comans EF, Joshi U, Semenza GL, Hoekstra OS, Lammertsma AA, et al. (2002). Biologic correlates of (18)fluorodeoxyglucose uptake in human breast cancer measured by positron emission tomography. *J Clin Oncol* **20**, 379–387.

[12] Ma WW, Jacene H, Song D, Vilardell F, Messersmith WA, Laheru D, Wahl R, Endres C, Jimeno A, Pomper MG, et al. (2009). [¹⁸F]fluorodeoxyglucose positron emission tomography correlates with Akt pathway activity but is not predictive of clinical outcome during mTOR inhibitor therapy. *J Clin Oncol* **27**, 2697–2704.

[13] Winiarska M, Bil J, Wilczek E, Wilczynski GM, Lekka M, Engelberts PJ, Mackus WJ, Gorska E, Bojarski L, Stoklosa T, et al. (2008). Statins impair antitumor effects of rituximab by inducing conformational changes of CD20. *PLoS Med* **5**, e64.

[14] Dimitroulakos J and Yeger H (1996). HMG-CoA reductase mediates the biological effects of retinoic acid on human neuroblastoma cells: lovastatin specifically targets P-glycoprotein-expressing cells. *Nat Med* **2**, 326–333.

[15] Allsopp RC, Lalo U, and Evans RJ (2010). Lipid raft association and cholesterol sensitivity of P2X1-4 receptors for ATP: chimeras and point mutants identify intracellular amino-terminal residues involved in lipid regulation of P2X1 receptors. *J Biol Chem* **285**, 32770–32777.

[16] Hinzpeter A, Fritsch J, Borot F, Trudel S, Vieu DL, Brouillard F, Baudouin-Legros M, Clain J, Edelman A, and Ollero M (2007). Membrane cholesterol content modulates CIC-2 gating and sensitivity to oxidative stress. *J Biol Chem* **282**, 2423–2432.

[17] Harikumar KG, Puri V, Singh RD, Hanada K, Pagano RE, and Miller LJ (2005). Differential effects of modification of membrane cholesterol and sphingolipids on the conformation, function, and trafficking of the G protein-coupled cholecystokinin receptor. *J Biol Chem* **280**, 2176–2185.

[18] Fantini J and Barrantes FJ (2009). Sphingolipid/cholesterol regulation of neurotransmitter receptor conformation and function. *Biochim Biophys Acta* **1788**, 2345–2361.

[19] Paila YD, Tiwari S, Sengupta D, and Chattopadhyay A (2011). Molecular modeling of the human serotonin(1A) receptor: role of membrane cholesterol in ligand binding of the receptor. *Mol Biosyst* **7**, 224–234.

[20] O’Malley MA, Helgeson ME, Wagner NJ, and Robinson AS (2011). The morphology and composition of cholesterol-rich micellar nanostructures determine transmembrane protein (GPCR) activity. *Biophys J* **100**, L11–L13.

[21] Baier CJ, Fantini J, and Barrantes FJ (2011). Disclosure of cholesterol recognition motifs in transmembrane domains of the human nicotinic acetylcholine receptor. *Sci Rep* **1**, 69.

[22] Kaliman P, Vinals F, Testar X, Palacin M, and Zorzano A (1995). Disruption of GLUT1 glucose carrier trafficking in L6E9 and Sol8 myoblasts by the phosphatidylinositol 3-kinase inhibitor wortmannin. *Biochem J* **312**(pt 2), 471–477.

- [23] Tchou J, Sonnad SS, Bergey MR, Basu S, Tomaszewski J, Alavi A, and Schnall M (2010). Degree of tumor FDG uptake correlates with proliferation index in triple negative breast cancer. *Mol Imaging Biol* **12**, 657–662.
- [24] Vander Heiden MG, Cantley LC, and Thompson CB (2009). Understanding the Warburg effect: the metabolic requirements of cell proliferation. *Science* **324**, 1029–1033.
- [25] Huang S and Czech MP (2007). The GLUT4 glucose transporter. *Cell Metab* **5**, 237–252.
- [26] Mahammad S, Dinic J, Adler J, and Parmryd I (2010). Limited cholesterol depletion causes aggregation of plasma membrane lipid rafts inducing T cell activation. *Biochim Biophys Acta* **1801**, 625–634.
- [27] Buhaescu I and Izzedine H (2007). Mevalonate pathway: a review of clinical and therapeutical implications. *Clin Biochem* **40**, 575–584.
- [28] Wang CY, Liu PY, and Liao JK (2008). Pleiotropic effects of statin therapy: molecular mechanisms and clinical results. *Trends Mol Med* **14**, 37–44.
- [29] Liao JK and Laufs U (2005). Pleiotropic effects of statins. *Annu Rev Pharmacol Toxicol* **45**, 89–118.
- [30] Ridker PM, Danielson E, Fonseca FA, Genest J, Gotto AM Jr, Kastelein JJ, Koenig W, Libby P, Lorenzatti AJ, MacFadyen JG, et al. (2008). Rosuvastatin to prevent vascular events in men and women with elevated C-reactive protein. *N Engl J Med* **359**, 2195–2207.
- [31] Freeman DJ, Norrie J, Sattar N, Neely RD, Cobbe SM, Ford I, Isles C, Lorimer AR, Macfarlane PW, McKillop JH, et al. (2001). Pravastatin and the development of diabetes mellitus: evidence for a protective treatment effect in the West of Scotland Coronary Prevention Study. *Circulation* **103**, 357–362.
- [32] Sattar N, Preiss D, Murray HM, Welsh P, Buckley BM, de Craen AJ, Seshasai SR, McMurray JJ, Freeman DJ, Jukema JW, et al. (2010). Statins and risk of incident diabetes: a collaborative meta-analysis of randomised statin trials. *Lancet* **375**, 735–742.
- [33] Preiss D, Seshasai SR, Welsh P, Murphy SA, Ho JE, Waters DD, DeMicco DA, Barter P, Cannon CP, Sabatine MS, et al. (2011). Risk of incident diabetes with intensive-dose compared with moderate-dose statin therapy: a meta-analysis. *JAMA* **305**, 2556–2564.
- [34] Guyton JR (2007). Niacin in cardiovascular prevention: mechanisms, efficacy, and safety. *Curr Opin Lipidol* **18**, 415–420.
- [35] Basso AD, Kirschmeier P, and Bishop WR (2006). Lipid posttranslational modifications. Farnesyl transferase inhibitors. *J Lipid Res* **47**, 15–31.
- [36] Weitz-Schmidt G, Welzenbach K, Brinkmann V, Kamata T, Kallen J, Bruns C, Cottens S, Takada Y, and Hommel U (2001). Statins selectively inhibit leukocyte function antigen-1 by binding to a novel regulatory integrin site. *Nat Med* **7**, 687–692.
- [37] Marcoff L and Thompson PD (2007). The role of coenzyme Q10 in statin-associated myopathy: a systematic review. *J Am Coll Cardiol* **49**, 2231–2237.
- [38] Haeuptle MA, Hulsmeier AJ, and Hennet T (2010). HPLC and mass spectrometry analysis of dolichol-phosphates at the cell culture scale. *Anal Biochem* **396**, 133–138.
- [39] Hillyard DZ, Jardine AG, McDonald KJ, and Cameron AJ (2004). Fluvastatin inhibits raft dependent Fcγ receptor signalling in human monocytes. *Atherosclerosis* **172**, 219–228.
- [40] Zhuang L, Kim J, Adam RM, Solomon KR, and Freeman MR (2005). Cholesterol targeting alters lipid raft composition and cell survival in prostate cancer cells and xenografts. *J Clin Invest* **115**, 959–968.
- [41] Maxfield FR and Tabas I (2005). Role of cholesterol and lipid organization in disease. *Nature* **438**, 612–621.
- [42] Simons K and Ikonen E (2000). How cells handle cholesterol. *Science* **290**, 1721–1726.
- [43] de Meyer F and Smit B (2009). Effect of cholesterol on the structure of a phospholipid bilayer. *Proc Natl Acad Sci USA* **106**, 3654–3658.
- [44] Thorens B and Mueckler M (2010). Glucose transporters in the 21st century. *Am J Physiol Endocrinol Metab* **298**, E141–E145.
- [45] Carruthers A, DeZutter J, Ganguly A, and Devaskar SU (2009). Will the original glucose transporter isoform please stand up! *Am J Physiol Endocrinol Metab* **297**, E836–E848.
- [46] Baker M (2010). Making membrane proteins for structures: a trillion tiny tweaks. *Nat Methods* **7**, 429–434.
- [47] Rasmussen SG, Choi HJ, Rosenbaum DM, Kobilka TS, Thian FS, Edwards PC, Burghammer M, Ratnala VR, Sanishvili R, Fischetti RF, et al. (2007). Crystal structure of the human β₂ adrenergic G-protein-coupled receptor. *Nature* **450**, 383–387.
- [48] Hiller S, Garces RG, Malia TJ, Orekhov VY, Colombini M, and Wagner G (2008). Solution structure of the integral human membrane protein VDAC-1 in detergent micelles. *Science* **321**, 1206–1210.
- [49] Epand RM, Thomas A, Brasseur R, and Epand RF (2010). Cholesterol interaction with proteins that partition into membrane domains: an overview. *Subcell Biochem* **51**, 253–278.
- [50] Kurowski MA and Bujnicki JM (2003). GeneSilico protein structure prediction meta-server. *Nucleic Acids Res* **31**, 3305–3307.
- [51] Kosinski J, Cymerman IA, Feder M, Kurowski MA, Sasin JM, and Bujnicki JM (2003). A “Frankenstein’s monster” approach to comparative modeling: merging the finest fragments of fold-recognition models and iterative model refinement aided by 3D structure evaluation. *Proteins* **53**(suppl 6), 369–379.
- [52] Parikh A, Childress C, Deitrick K, Lin Q, Rukstalis D, and Yang W (2010). Statin-induced autophagy by inhibition of geranylgeranyl biosynthesis in prostate cancer PC3 cells. *Prostate* **70**, 971–981.